AT&T Technical Journal
Vol. 64, No. 10, December 1985
Printed in U.S.A.

Statistical Model for Amplitude and Delay of Selective Fading

By P. BALABAN*

(Manuscript received September 11, 1985)

The transmission performance of digital radio systems is controlled by spectral distortion caused by multipath fading. To evaluate this performance for digital systems with high-order modulation schemes, a statistical model for frequency-selective fading is needed. New propagation data obtained in Gainesville, Florida, were used to generalize Rummler's model to include group delay response. The introduction of the delay response data into the model of the fading channel enabled the classification of the fades as minimum phase and nonminimum phase. We found that 24 percent of all fades have significant delay distortion, and can be characterized as being minimum phase or nonminimum phase. In the range of practical interest, there are as many minimum phase as nonminimum phase fades. The results of this work will facilitate a better understanding of the fading channel, which will be beneficial in the engineering of radio routes and digital radio design. The results also demonstrate the need for a description of the geographical occurrence of dispersion, which will differ from that for multipath fading at a single frequency. This is based on the observation, presented in this paper, that the relative amount of dispersive fading is significantly greater in Gainesville, Florida, than in Palmetto, Georgia. The availability of a dispersive fading map will facilitate the accurate engineering of digital radio routes.

I. INTRODUCTION

Digital radio communication systems are sensitive to selective fading. To evaluate their performance, a statistical model for frequency-

* AT&T Bell Laboratories.

selective fading is needed. Although the amplitude response of multipath fading in a microwave communication channel has been extensively modeled previously,[1–8] statistically based results for the group delay response were not available until recently,[9–11] and work on modeling the delay in a fading channel is just beginning.[12]

A successful model for multipath fading using amplitude data was developed by W. D. Rummler.[3,4] The delay response in this model was inferred from the measured amplitude. This led to an ambiguity, since both minimum phase and nonminimum phase fades are possible. In this paper, we generalize the use of this model by including group delay data. The model parameters are defined to characterize both minimum phase and nonminimum phase behavior, and statistical distributions of these parameters are compiled. Rummler's model, although developed for data obtained in the Palmetto experiment for a 6-GHz carrier with a 25.3-MHz bandwidth, has proven itself robust and applicable for a wide range of frequencies. Our new results are based on amplitude and delay measurements at 6 GHz in a 30-MHz bandwidth over a 23.3-mile path between Gainesville and Sparr, Florida.

Inclusion of the delay response into the statistical model of the dispersive line-of-sight channel will benefit both the engineering of digital radio routes and digital radio equipment design. The description of the occurrence of events with minimum and nonminimum phase response is of immediate practical interest. The need for delay description, such as provided by our model, will increase with the growth of sophistication of digital radio.

The experiment and the modeling procedures are described in Section II. The selection of the scans recorded by the instrumentation is outlined and the fixed delay Rummler model for selective fading[3] is described. It is shown that, by appropriately redefining the parameters of this model, it is suitable for characterization of amplitude and delay.

Section III presents the statistical distributions of the modified model parameters for the data measured in Gainesville. Comparison with Palmetto data have been made that show that the Gainesville fading is more dispersive than that at Palmetto.

II. CHARACTERIZATION AND MODELING

2.1 The experiment

The Gainesville experiment is implemented on a 23.3-mile path between Gainesville and Sparr, Florida, in a 6-GHz channel with a 30-MHz bandwidth. The experimental setup is described elsewhere.[9,13] The amplitude and delay characteristics of the faded link are measured by a Wandel-Goltermann link analyzer and recorded on magnetic

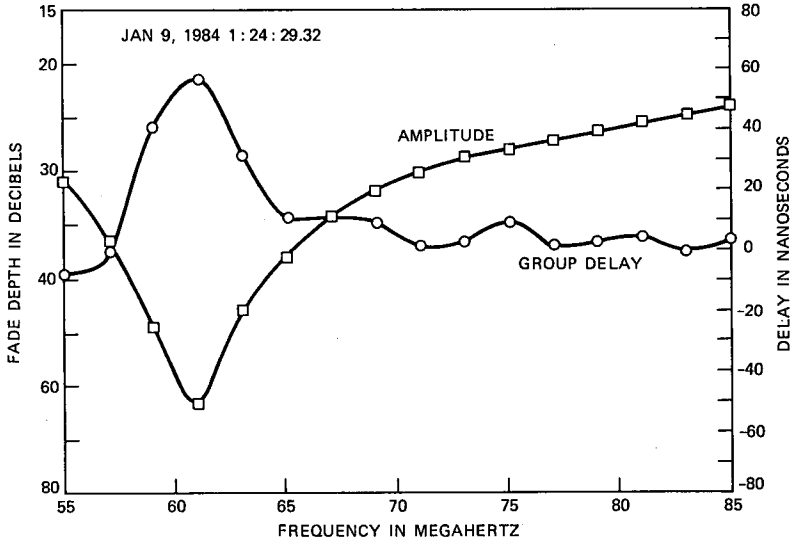

Fig. 1—A typical scan of a fading event.

tape. The amplitude and delay were measured during alternating frequency scans. Each scan duration was 0.1 second followed by a 0.1-second retrace. A measurement period was thus 0.4 second. The amplitude scale was set up for fades between 15 to 65 decibels and the delay between ±50 nanoseconds.* Amplitude fades smaller than 15 decibels were out of scale and recorded at 1 scan/min. Each scan was sampled at intervals of 2 MHz or 16 samples over the 30-MHz bandwidth.

The database used for this study consists of approximately 43,000 scans that represent 17,000 seconds of fading activity. The data were recorded in Gainesville for 11 months during the period from 1982 through 1984.

2.2 Selection of data for modeling

A fading event recorded in Gainesville is shown in Fig. 1. As a rule, fading events were slow enough to be considered static during the frequency scan. Although on some scans a certain amount of distortion that could be attributed to the dynamics of the system was noticeable, it was small enough to be negligible. Many scans were incompletely recorded because of the limited range of both amplitude and delay measurement equipment. Therefore, the recorded fading scans were first screened in order to eliminate fading scans that are not suitable

* Modified to ±100 nanoseconds in February 1985.

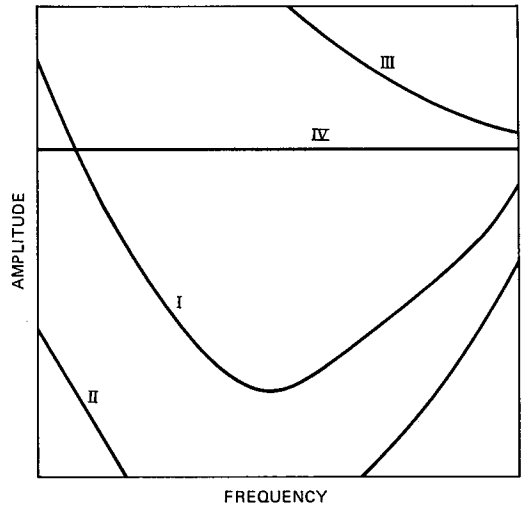

Fig. 2—Complete and incomplete amplitude scans. Scans II and III rejected. Scan IV marked.

for modeling. In addition, scans that do not need dispersive modeling, but have to be included in the total fading statistics, were identified during the screening process. This screening was done as follows.

A. Only those responses recorded at a rate of 2.5 scans/s were selected for processing. Responses recorded at different rates were regarded as unfaded.

B. Data scans were categorized on the basis of amplitude response. Figure 2 shows several amplitude scans as they appear in the recorded data. Only complete scans of types I and IV were modeled. Type II was rejected because part of the scan is out of scale at the high end (>65 dB). This is a rare event; about 30 such scans were recorded. Type III was eliminated because the trace is out of scale at the low end (<15 dB). This is the most common type that was eliminated; about 20 percent of all scans were type III. Flat fades of type IV were marked to indicate that dispersive modeling is not required.

C. Data scans were also categorized on the basis of delay response. Figure 3 shows several delay scans. Scans of types I and II were included as they are. Flat delay scans of type III that have a dispersive amplitude response were marked to indicate that delay modeling is not required. Scans of types IV and V are incomplete and were marked so that they can be modeled using an alternate technique.

Accordingly, 51,953 scans were selected using criterion A. From these, 9103 were eliminated because the amplitude was out of scale; 16,892 were marked because the amplitude was flat; 13,580 were marked because the delay was flat; and 2269 were marked because the

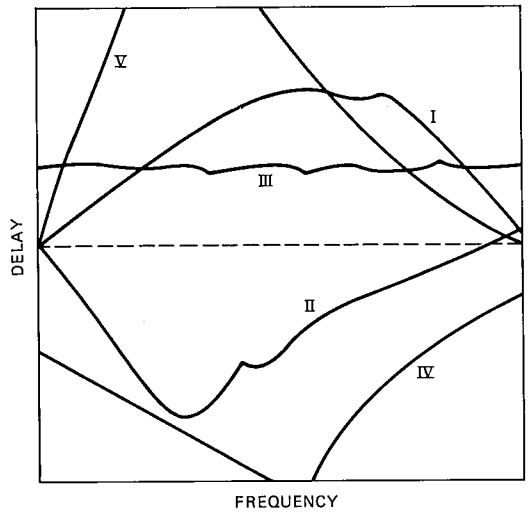

Fig. 3—Complete and incomplete delay scans. Scans III, IV, and V marked.

delay was out of scale. Consequently, 12,538 scans, or 24 percent of the total, had sufficient delay information to be modeled using both the delay and amplitude measurements. For the rest, only the amplitude measurements were used.

2.3 The model

The modeling was done using Rummler's model for selective fading.[3] In addition to wide acceptance and extensive validation this model has the advantage of separating the flat component of the fade from the dispersive component. The dispersive component can thus be statistically characterized by one parameter. The transfer function of the model is

$$H(\omega) = a(1 - be^{-j(\omega-\omega_0)\tau}), \tag{1}$$

where we can regard τ as the relative path delay of the second ray, b and $\omega_0\tau$ the relative amplitude and phase of that ray, and a as the amplitude scale factor.

The squared amplitude (or power) response is

$$Y(\omega) = |H(\omega)|^2 = a^2[1 + b^2 - 2b\cos(\omega - \omega_0)\tau]; \tag{2}$$

and the group delay is

$$D(\omega) = -\frac{d\phi(\omega)}{d\omega} = \tau\frac{b(b - \cos(\omega - \omega_0)\tau)}{1 + b^2 - 2b\cos(\omega - \omega_0)\tau}. \tag{3}$$

The delay parameter τ is constant in this model, at $\tau = 6.25$ ns. Typical

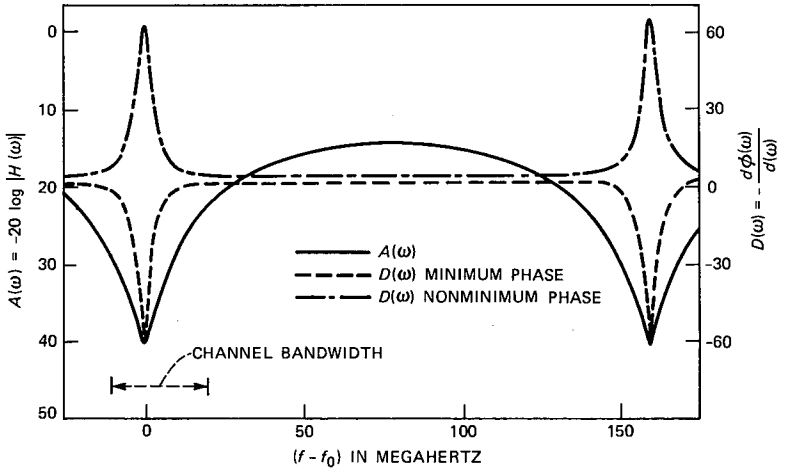

Fig. 4—Amplitude and delay characteristics of the fading model channel response: $a_1 = 0.1$, $b_1 = 0.9$, $a_2 = 0.09$, and $b_2 = 1.111$.

amplitude and delay frequency responses based on eqs. (2) and (3) are shown in Fig. 4.

Although the model was developed using measured amplitude data only, we found it adequate for modeling of selective fading using both measured amplitude and group delay data. The statistical distribution of the parameters naturally differs from those obtained for amplitude only, because we can distinguish between minimum and nonminimum phase scans.

2.4 Fitting the model to the amplitude data

The model parameters were estimated by fitting the squared amplitude in eq. (2) to the measured amplitude responses. The estimation procedure followed was similar to the one described by Rummler in Ref. 3. From eq. (2) it is clear that

$$Y(\omega) = \alpha - \beta \cos(\omega - \omega_0)\tau, \tag{4}$$

where

$$\alpha = a^2(1 + b^2) \tag{5a}$$

$$\beta = 2a^2b. \tag{5b}$$

For convenience, the channel scan is measured in frequency increments of 2 MHz, resulting in 16 samples over the 30-MHz range

$$\omega_n = 2\pi f_n = 2\pi n(2 \cdot 10^6); \qquad n = 1, 16. \tag{6}$$

If we choose

$$\tau = \frac{1}{M(2 \cdot 10^6)}, \tag{7}$$

then the phase increments are

$$\omega_n \tau = 2\pi \frac{n}{M}. \tag{8}$$

Choosing $M = 80$, the delay is $\tau = 6.25$ ns. Thus the in-band frequencies correspond to n values between 1 and 16, and the model transfer function is periodic with $M = 80$, which corresponds to a frequency period $1/\tau = 160$ MHz (see Fig. 4).

The first modeling step is to choose α, β and ω_0 so that the sequence of measured values $\{Y_n\}$, $n = 1, 16$, is closely matched by the sequence $\{Y(\omega_n)\}$ using eqs. (4) and (8). Estimates of α, β and ω_0 were found by minimizing the mean square error, E_{rms}, between these sequences. We define E_{rms} as

$$E_{\text{rms}} = \frac{\sum_{n=1}^{16} C_n (Y_n - Y(\omega_n))^2}{\sum C_n}, \tag{9}$$

where C_n is a weighting coefficient. Since Y_n is derived from data that was uniformly quantized on a logarithmic scale, we use a weighting that is approximately logarithmic. Hence,

$$C_n = \frac{1}{Y_n^2}. \tag{10}$$

A measure of the goodness of this fitting for a given scan is the root-mean-square value of the decibel error over the sampled frequencies, i.e.,

$$E_{\text{dB}} = \left[\frac{1}{16} \sum_{n=1}^{16} (Y_n[\text{dB}] - Y(\omega_n)[\text{dB}])^2\right]^{1/2}. \tag{11}$$

A plot of the distribution of this error for the total population is shown in Fig. 5. As seen from the plot, nearly 99.9 percent of the errors are below 2 dB.

The second step in the modeling is to find a and b given estimates for α and β. From these estimates the parameters a and b are obtained by inverting eq. (5). The set $[a, b]$ has two possible solutions $[a_1, b_1]$ and $[a_2, b_2]$

$$b_1 = \frac{\alpha}{\beta} - \left[\left(\frac{\alpha}{\beta}\right)^2 - 1\right]^{1/2}$$

$$a_1 = \left[\frac{\beta}{2b_1}\right]^{1/2}, \tag{12a}$$

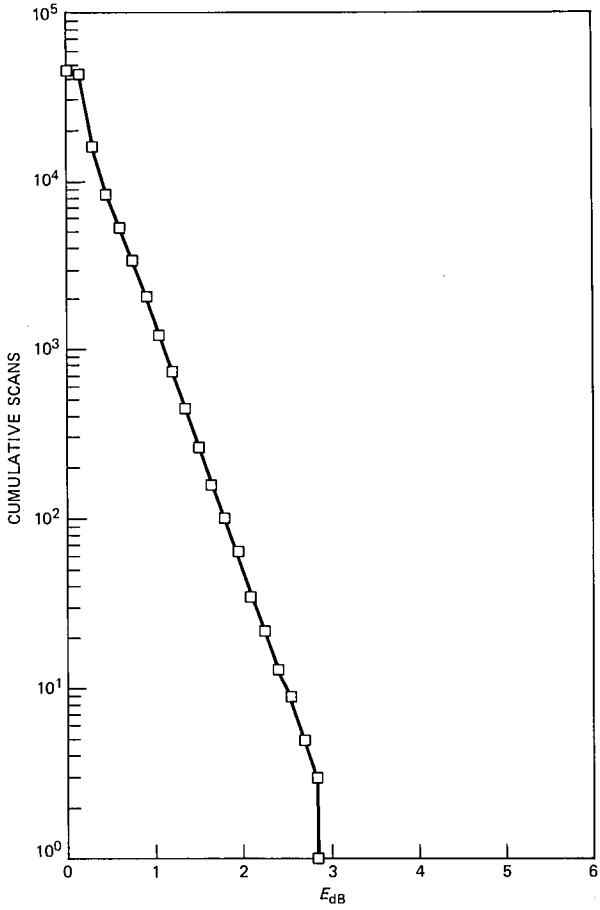

Fig. 5—Distribution of the root-mean-square error of the amplitude fit.

and

$$b_2 = \frac{\alpha}{\beta} + \left[\left(\frac{\alpha}{\beta}\right)^2 - 1\right]^{1/2}$$

$$a_2 = \left[\frac{\beta}{2b_2}\right]^{1/2}. \tag{12b}$$

It is clear from eq. (4) that $\alpha \geq \beta$ in every scan, since $Y(\omega)$ must fit a sequence of nonnegative powers. Thus, both solutions for b are real. It also follows that $b_1 b_2 = 1$.

The two solutions in eqs. (12a) and (12b) satisfy the amplitude response fit. The solution $[a_1, b_1]$ where $b_1 < 1$ corresponds to a minimum phase transfer function, since it produces a zero in the left

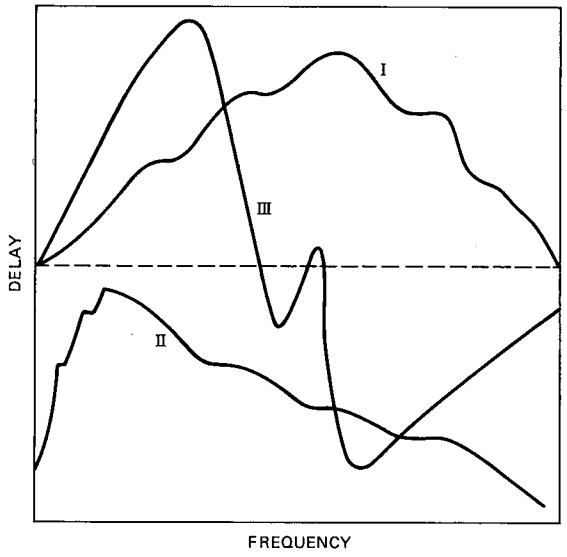

Fig. 6—Fading delay scans.

half of the complex frequency plane, and the solution $[a_2, b_2]$, where $b_2 > 1$ corresponds to a nonminimum solution, since it produces a zero in the right half of that plane.

The decision of whether a given scan corresponds to a minimum phase or nonminimum phase fade is made here by using the delay data. For a substantial fraction of the available data, the delay response was flat. For this population, the estimations were done by using amplitude data only and assuming the minimum phase solution.

2.5 Fitting the model to the delay data

2.5.1 Typical delay data

Figure 6 shows a few typical delay scans. To determine whether a scan is minimum phase or nonminimum phase, we have to examine the shape of the delay response. Scan I shows clearly a nonminimum phase delay shape, but so does scan II, although it is negative. The group delay scans usually exhibit a constant delay offset that has to be subtracted during the fitting process. Scan III is caught in the transition between minimum phase and nonminimum phase; this sometimes happens at very deep fades.

The usual time trajectory of a deep fade is as follows: The fade appears as a minimum phase fade, gradually deepens, crosses to a nonminimum phase fade, then becomes shallower, and disappears. It usually does not cross back to the minimum phase shape.

2.5.2 The fitting procedure

Each delay scan is sandwiched between two amplitude scans that are separated by 0.2 second. The initial parameters ω_{0i}, b_{1i} and b_{2i} used to fit each delay scan [eq. (3)] were interpolated from the two amplitude scans. Two error estimates were then set up, namely,

$$E_1 = \frac{1}{16} \sum_{n=1}^{16} [D_n(b_1, \omega_0) - (\hat{D}_n - D_0)]^2, \tag{13}$$

and

$$E_2 = \frac{1}{16} \sum_{n=1}^{16} [D_n(b_2, \omega_0) - (\hat{D}_n - D_0)]^2,$$

where $D_n(b_1, \omega_0)$ is the minimum phase delay response, and $D_n(b_2, \omega_0)$ the nonminimum phase delay response, as derived by fitting the amplitude data. Further, $\hat{D}_n$ is the measured group delay at frequency ω_n. The group delay scans usually exhibit an unknown constant delay offset D_0 (see Fig. 6, scan II) that has to be estimated during the fitting process.

The above errors were minimized using a quasi-Newton optimization algorithm. First, E_1 and E_2 were minimized with respect to the delay offset D_0. By selecting the response with the better fit, this step was sufficient to decide if the shape is minimum phase or nonminimum phase. The delay responses thus obtained usually fit within a 7-ns root-mean-square error, for scans having swings smaller than 50 ns. The delay response fits were further optimized, by adjusting the parameter b, to yield root-mean-square errors smaller than 4 ns. These further optimization did not change the values of b significantly. The E_{dB} values [eq. (11)], of the resulting amplitude fits changed by less than 1 dB.

Delay scans with swings larger than 50 ns were out of scale and could not be fitted.* For these scans, the choice between minimum phase and nonminimum phase was made by minimizing the error with respect to the offset D_0 only. The initial parameters, interpolated from the adjacent amplitude scans, were used in the statistics.

One type of poor fit occurred when a delay scan was in a transition from minimum phase to nonminimum phase. These scans were eliminated from the modeling.

The delay data could not be fitted more tightly to the model because, as seen from Fig. 7, the residuals have strong harmonic components. The harmonic components indicate long delay echos in the system. We have concluded from our experiments that this distortion is caused

* The instrumentation was changed recently to record delays in the range of ±100 ns.

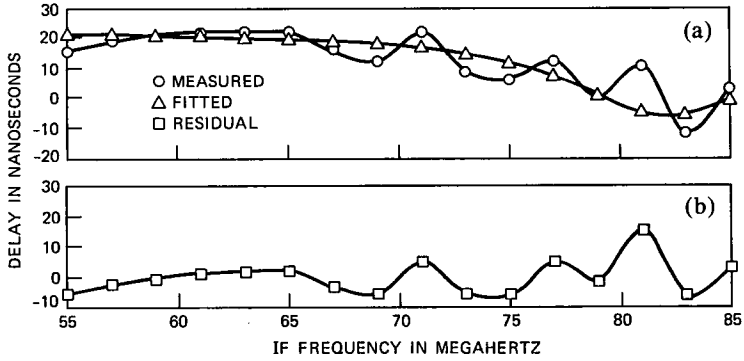

Fig. 7—(a) Measured and fitted delay curves. (b) Delay residual.

by multimoding in the antenna and waveguide system of the transmitter and receiver.

III. STATISTICAL DISTRIBUTIONS OF MODEL PARAMETERS

The statistical distributions for the parameters of the fading model transfer function in eq. (1) were characterized previously using amplitude response data from the Palmetto experiment.[3,4] We used a similar approach to generate parameter distributions for the present case. Essentially, the data scans can be divided into four distinct groups: Minimum-phase fades, nonminimum phase fades, flat amplitude fades and flat delay fades. These four groups are characterized best if the estimated statistical distributions of the model parameters are described separately. The flat amplitude and flat delay groups are degenerate cases, where only limited modeling was required. A scan with a flat amplitude response has also a flat delay response. However, a flat delay scan does not necessarily correspond to flat amplitude response. Since the delay notch is narrower than the amplitude notch (see Fig. 4), many scans with a sloping amplitude response, corresponding to an out-of-band notch, have flat delays (see Section 3.5).

The statistical characterizations of the minimum phase fades and nonminimum phase fades are done first, followed by the characterizations of the flat amplitude and flat delay fades. The statistical distributions of the model parameters for the whole fading population are estimated next, based on amplitude data only. This is done in order to compare the fading characteristics of the Gainesville channel with those of the Palmetto channel.

3.1 Minimum phase fades

For minimum phase fades the distributions are generated for the parameters

$$\omega_0$$

$$A_1 = -20 \log a_1$$

$$B_1 = -20 \log(1 - b_1), \tag{14}$$

where a_1 and b_1 are the minimum phase solutions of eq. (12a), ω_0 is the notch frequency, B_1 is the relative notch depth in decibels and A_1 is the amplitude scale factor in decibels.

3.2 Nonminimum phase fades

For nonminimum phase fades, the parameter b_2 is unbounded and is not easily characterized. Equation (1) is then rewritten as

$$H(\omega) = a_2 b_2 (e^{-j(\omega-\omega_0)\tau} - 1/b_2), \tag{15}$$

and we define

$$B_2 = -20 \log(1 - 1/b_2)$$

$$A_2 = -20 \log(a_2 b_2). \tag{16}$$

As shown below, the choice of these parameters leads to distributions very similar to those of their minimum phase counterparts.

3.3 Distributions for minimum phase and nonminimum phase fades

3.3.1 The distributions of B_1 and B_2

The cumulative distributions of B_1 and B_2 are shown in Fig. 8. The abscissa is B_1 or B_2 in decibels, and the ordinate shows the time T that B_1 or B_2 is greater than the abscissa. It is clearly seen that, if we ignore the fades with low dispersion ($B \leq 8$ dB) and assume that the data above 30 dB have too few samples to be reliable, the two curves can be fitted to within ±1.75 dB by one exponential distribution. This distribution is

$$T = 1.37 \cdot 10^4 \, e^{-\frac{B}{4.82}} = 1.37 \cdot 10^4 \, L^{1.8}, \qquad \text{for} \quad 8 \leq B \leq 30 \text{ dB}, \tag{17}$$

where $L = 10^{\frac{-B}{20}}$, and represents the minimum fading voltage relative to the amplitude scale factor a_1 (or $a_2 b_2$).

As seen from Fig. 8, there are overall more minimum phase than nonminimum phase fades (58 percent). However, if we restrict ourselves to the practically significant range of $8 \leq B \leq 30$ dB, the proportion of nonminimum phase fades is 50 percent. Both the minimum and nonminimum phase fades distributions can be expressed, within the limits of the approximation, in eq. (17).

3.3.2 The distribution of the parameters A_1 and A_2

The cumulative time distributions for A_1 and A_2 are shown in Fig.

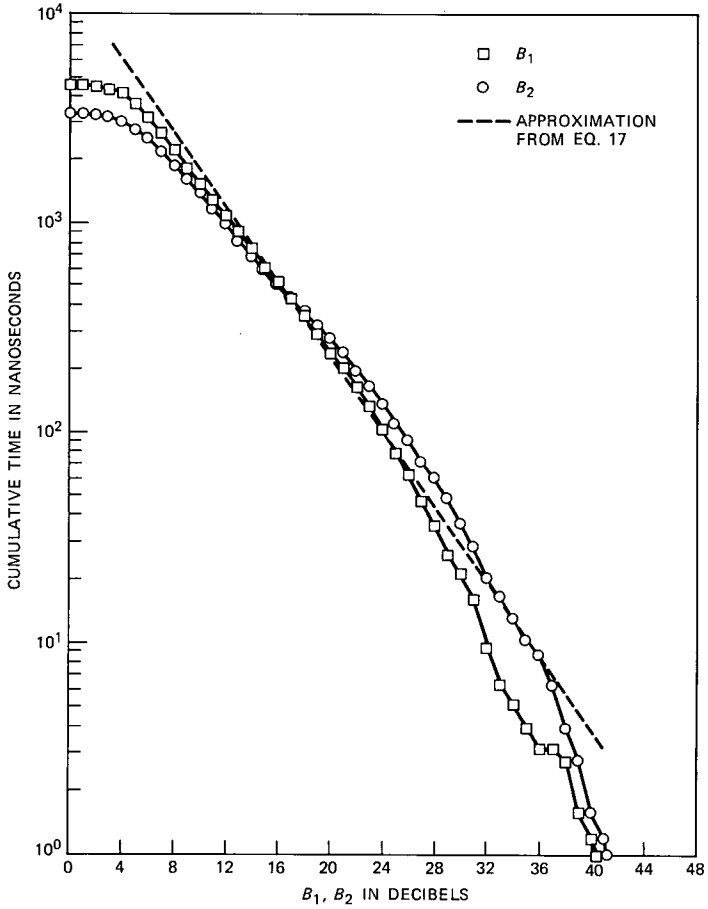

Fig. 8—Distribution of parameters B_1 and B_2.

9. It is clearly seen that the two distributions are almost identical for larger A (above 14 dB). The means and standard deviations are

$$\bar{A}_1 = 15 \text{ dB}, \qquad \sigma_1 = 3.0 \text{ dB}$$
$$\bar{A}_2 = 15.5 \text{ dB}, \qquad \sigma_2 = 3.0 \text{ dB}. \tag{18}$$

The unnormalized probability density functions (pdf's) of A_1 and A_2 are shown in Fig. 10. (These pdf's are scaled in such a way that the ordinate displays on a logarithmic scale the number of seconds that A was within ±0.5 dB of the abscissa. This same format is used in all the pdf's shown later.) The pdf's show a definite asymmetry about the mean. This deviation from a Gaussian distribution* could be

* A was Gaussian for the Palmetto data.

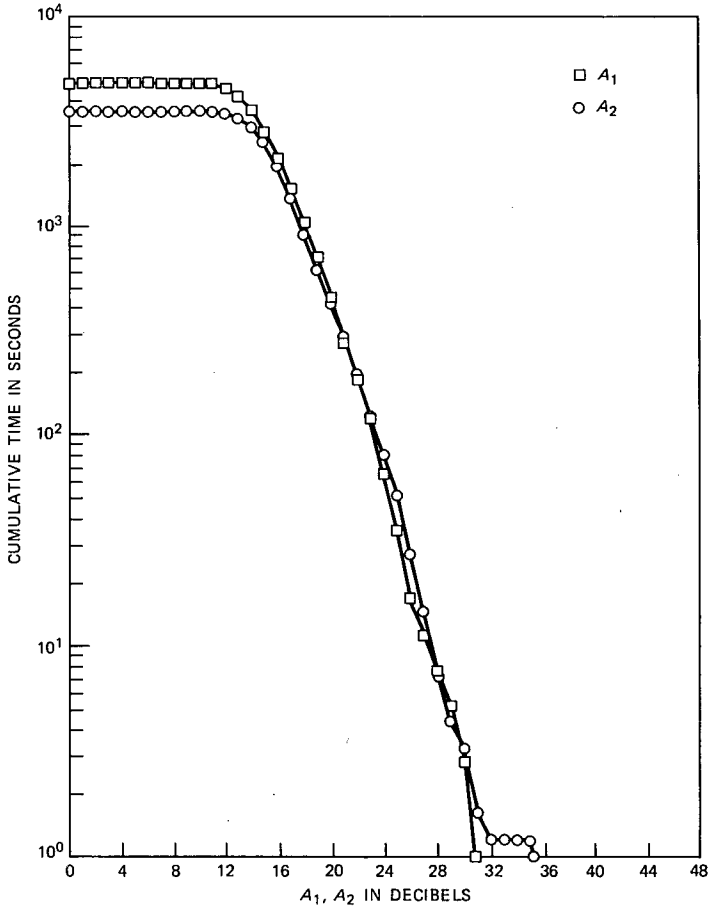

Fig. 9—Distribution of parameters A_1 and A_2.

partially attributed to the data gathering method used in Gainesville (see Section 2.2).

The means and standard deviations of A_1 and A_2 as functions of B_1 and B_2 are shown in Fig. 11. These plots show clearly that the parameters A and B are uncorrelated for the Gainesville data.*

3.3.3 Possible discrepancies in the A and B distributions caused by instrumentation

1. The amplitude and delay characteristics were sampled every 2 MHz by the recording equipment over the 30-MHz frequency scan.

* A and B were correlated for the Palmetto data.

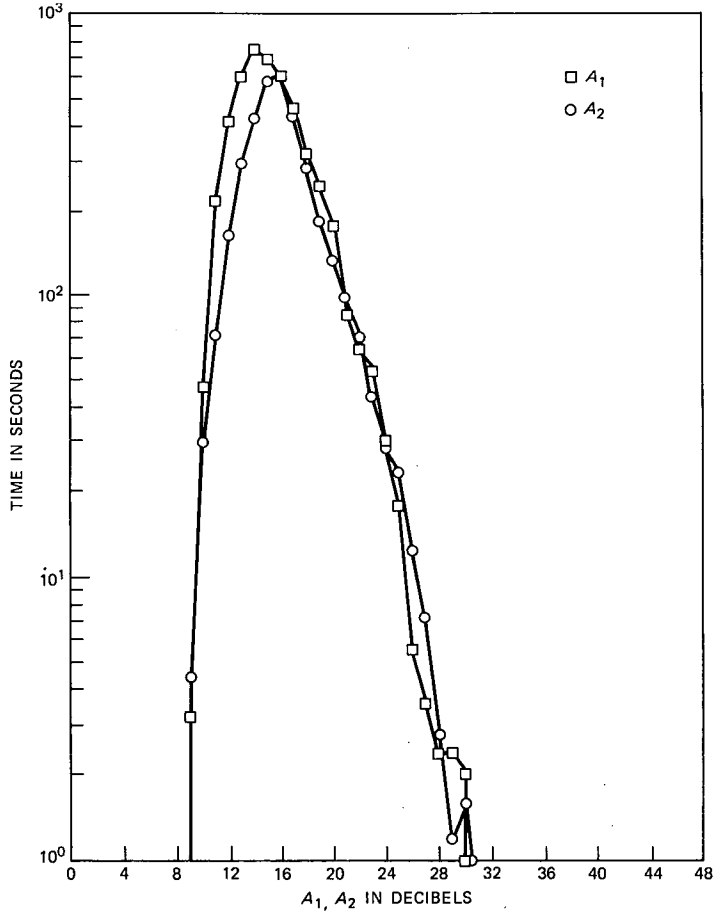

Fig. 10—Unnormalized probability density functions of A_1 and A_2.

The 2-MHz resolution may be too low for very deep dispersive fades, and cause flattening of these curves during the fitting process. This may cause the distributions of B_1 and B_2 to appear steeper for very large B values than they really are.

2. The Microwave Link Analyzer (MLA) was set up to measure amplitudes between 15 to 65 dB only. Therefore, some of the shallow fading events with small A and small B are not recorded. This could cause the distribution of B for small values to appear flatter than they really are, and the distributions of A to appear less symmetric.

3.3.4 The distribution of the notch frequency ω_0

Figure 12 shows the density function of the notch frequency, for both the minimum and nonminimum phase fades, as estimated by the

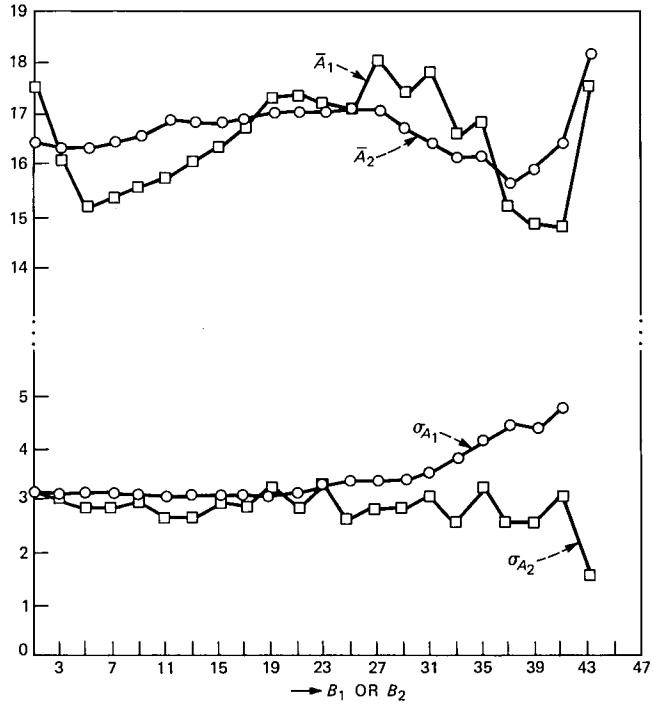

Fig. 11—Mean and standard deviation of $A_1(A_2)$ as functions of $B_1(B_2)$.

modeling procedure. This model estimates that approximately 70 percent of the scans have an in-band notch. This is to be expected because, as seen from Fig. 4, the delay shape is steeper and narrower than the amplitude notch. Therefore, most of the scans that have an in-band slope (out-of-band notch) have a flat delay response, and are therefore not characterized in this group (see Section 2.2).

Fitting the model to amplitude shapes that have in-band slopes is not unique, since small perturbations in data can produce large variations of out-of-band notch depth and frequencies. The modeling algorithm in its present form has a tendency to move the notch for slope shapes close to the edges of the band. We have tried, with variable success, to use also the delay data in placing the out-of-band notches. However, the delay data for shapes with out-of-band notches are limited and heavily corrupted with multimode distortion that made the fitting of the model rather difficult.

3.4 Statistical distribution of flat-amplitude fades

Amplitude scans that were flat within 1 dB were assumed to be nondispersive. For such scans, therefore, A was the only parameter

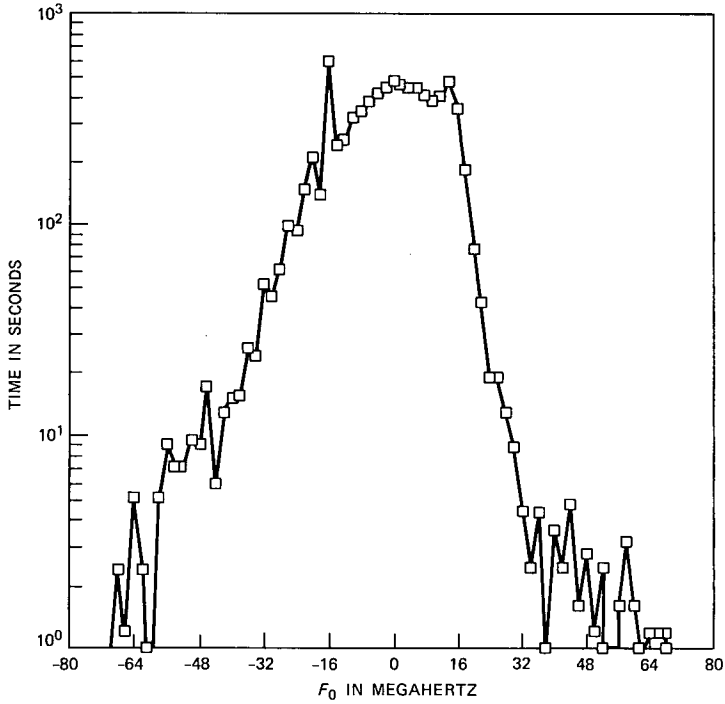

Fig. 12—Unnormalized probability density function of the notch frequency F_0, measured from midband.

modeled. The cumulative distribution of A for this case is shown in Fig. 13. As in previous cases, the distribution exhibits a truncated Gaussian behavior, with

$$\bar{A} = 15.9 \text{ dB}, \qquad \sigma = 2.85 \text{ dB}. \tag{19}$$

3.5 Statistical distribution of flat-delay fades

Scans that did not have a flat amplitude but exhibit a small delay distortion, $D(\omega)_{\text{peak to peak}} \leq 7$ ns, were regarded as having a flat delay. Scans of this type can be put into two categories:

(a) Scans with in-band, or close to in-band, notches and small amplitude deviations. A 7-ns delay notch corresponds to an amplitude notch with $B = 6.5$ dB.

(b) Scans with amplitude slopes that may have a notch so far out of band that the delay distortion is negligible.

In both of the above cases the delay information is too limited to be used to decide whether the scan is minimum phase or nonminimum phase. Since it is relatively unimportant to differentiate, in these

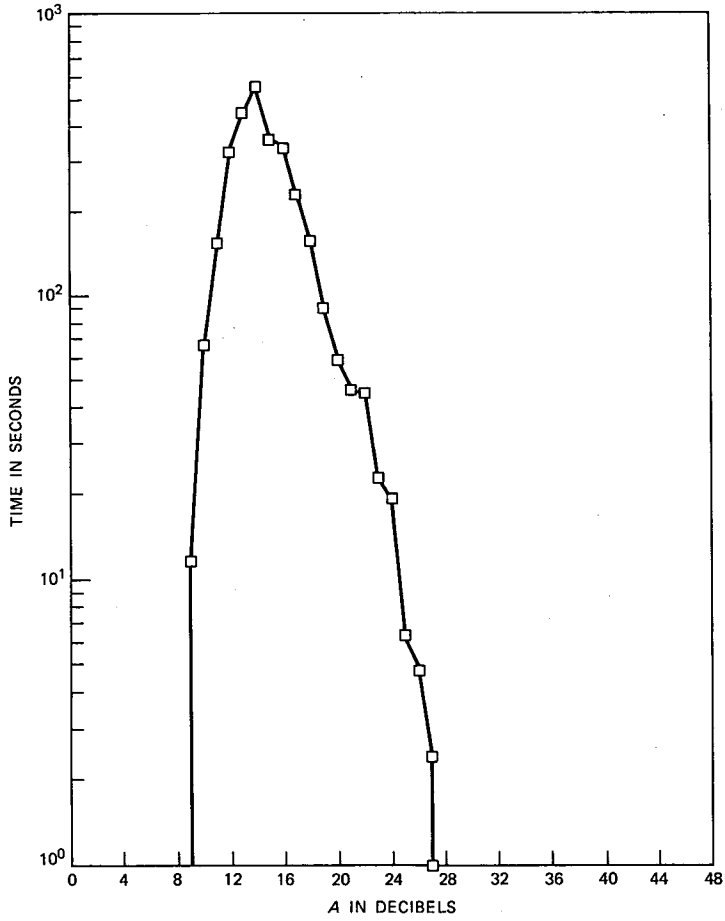

Fig. 13—Unnormalized probability density function of A for flat amplitude fades.

cases, between minimum phase and nonminimum phase fades, the statistics described below were compiled as though all such fades were minimum phase.

Figure 14 shows the distribution of B. As seen from the plot, 96 percent of the scans have $B \leq 6.5$ dB, which puts them in the category (a) above. Only 4 percent belong to category (b).

Figure 15 shows the probability density of A, wherein

$$\bar{A} = 15.8 \text{ dB}, \qquad \sigma = 2.6 \text{ dB}. \tag{20}$$

3.6 Parameter distributions for the total fade population and comparison with Palmetto

The distributions of the model parameters for the whole fade population, derived entirely from amplitude response data and comprising

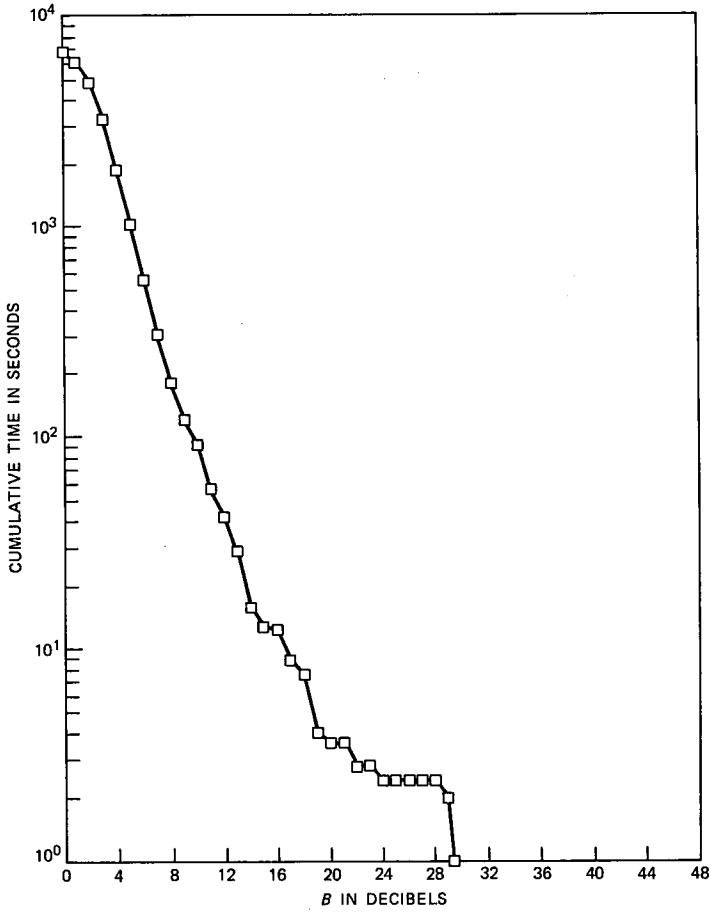

Fig. 14—Distribution of B for flat delay fades.

the four groups characterized in previous sections, are described below. By ignoring the delay characteristics, we computed the model parameters as if all fades were minimum phase. This was done in order to have a basis for comparison with the results obtained in the Palmetto experiment.

3.6.1 B distributions

Figure 16 shows the distribution of the parameter B, as measured in Gainesville. Within reasonable accuracy the distribution can be modeled by the exponential curve

$$T = 2.37 \cdot 10^4 \, e^{-\frac{B}{5}} = 2.37 \cdot 10^4 \, L^{1.72}. \tag{21}$$

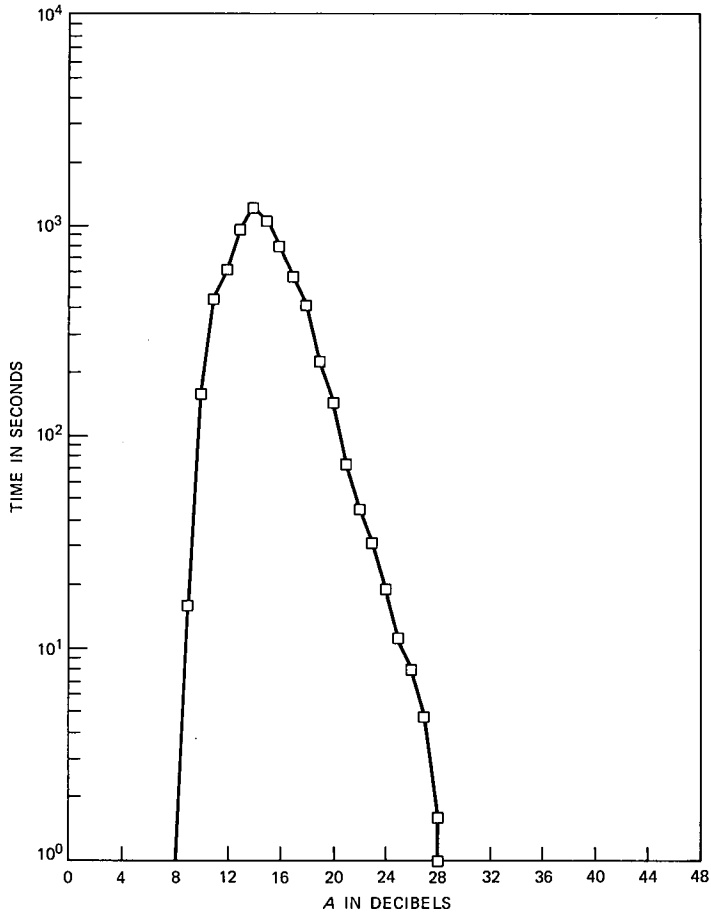

Fig. 15—Unnormalized probability density function of A for flat delay fades.

The fading data were recorded for 11 months, well distributed over all seasons during 1.5 years in 1982–1984. The curve in Fig. 16 can therefore be regarded as an annual average distribution of dispersive fading in Gainesville. The other curve in Fig. 16 shows the annual distribution of B for the Palmetto data. This distribution was extrapolated from data measured in Palmetto in 1977.[4] The total fading for the heaviest month of the year was estimated to be 8000 seconds, where the total fading was defined as the intercept of the B distribution with the $B = 0$ axis. To approximate the average annual fading in Palmetto, we multiplied the seconds for the heaviest fading month by a scale factor of 3.5. The average annual fading in Palmetto was thus estimated to be 28,000 seconds.

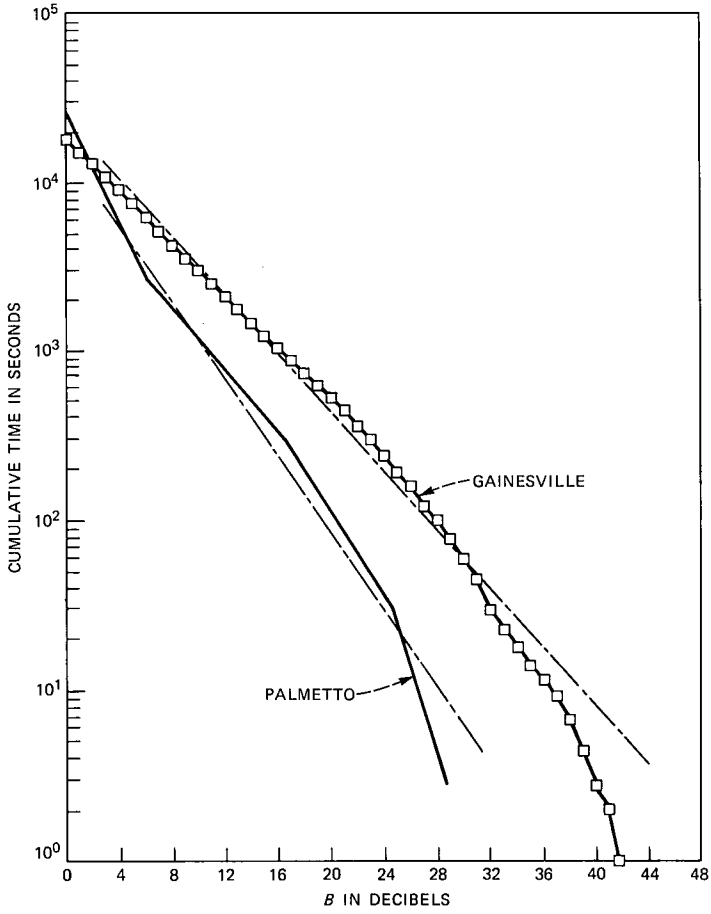

Fig. 16—Average annual probability distributions for B for the total populations of Gainesville and Palmetto.

The Palmetto distribution is steeper than that for Gainesville and can be modeled over its central region by

$$T = 1.6 \cdot 10^4 \, e^{-\frac{B}{3.8}} = 2 \cdot 10^4 \, L^{2.28}, \qquad 4 \text{ dB} \leq B \leq 25 \text{ dB}. \quad (22)$$

It can be surmised from the shape of the Gainesville distribution that fading on that path is more dispersive than the Palmetto fading. By examining, for illustration purposes, the total dispersive fading for $B \geq 20$ dB, we see from Fig. 16 that there is five times more of it in Gainesville than in Palmetto.

3.6.2 A distributions

Figure 17 shows the probability density function of parameter A. It has a truncated Gaussian shape, with mean and standard deviation

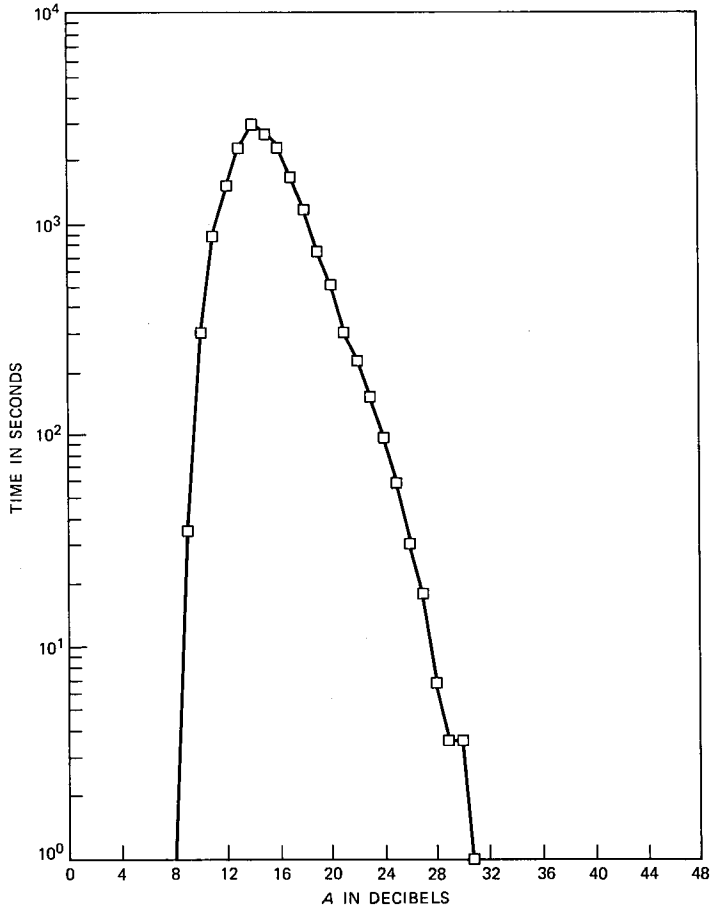

Fig. 17—Unnormalized probability density function of A for the total population.

$$\bar{A}_G = 16.2 \text{ dB}; \qquad \sigma_G = 2.85 \text{ dB}. \tag{23}$$

The corresponding distribution in Palmetto was Gaussian, with mean and standard deviation

$$\bar{A}_P = 25 \text{ dB}; \qquad \sigma_P = 5 \text{ dB}. \tag{24}$$

Moreover, the mean $\bar{A}_P$ was correlated with B_P in the Palmetto experiment. The Gainesville parameters $\bar{A}_G$ and B_G are independent (Fig. 18).

The apparent truncation of the A distribution is probably due to the data gathering method in Gainesville. Specifically, fades below 15 dB were not recorded. This could also be a reason why A and B are uncorrelated in Gainesville. In Palmetto, $\bar{A}$ was correlated with B, for $B < 10$ dB only.

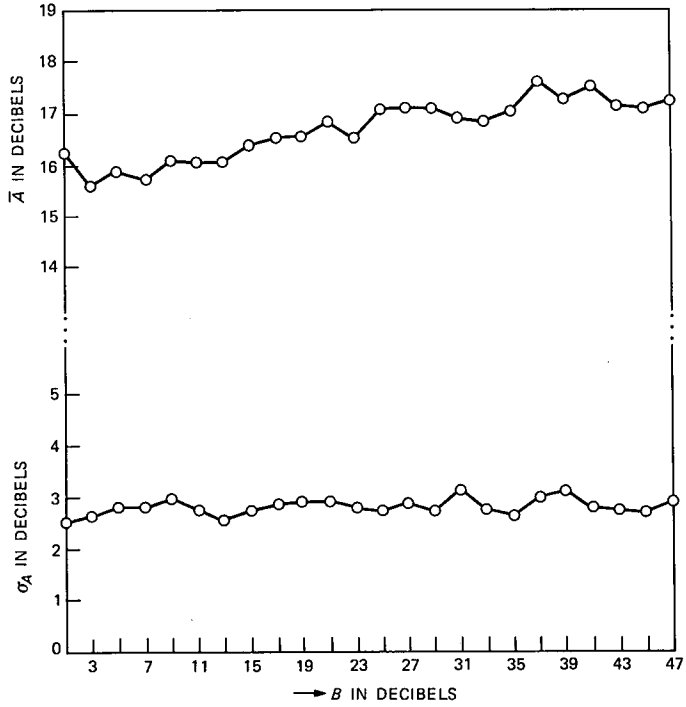

Fig. 18—Mean and standard deviation of A as functions of B.

3.6.3 Distribution of notch frequency ω_0

The probability density function of the notch frequency for the total fade population is shown in Fig. 19. Most of the scans have an in-band notch (55 percent). The notch frequency does not exhibit the bimodal distribution shown in Palmetto.

IV. CONCLUSION

4.1 Summary

The fading data obtained in the Gainesville experiment were for both amplitude and group delay. We generalized the method of Rummler[3,4] to include group delay response data, and thus obtain both minimum phase and nonminimum phase model parameters.

The distributions for minimum phase and nonminimum phase fades can be regarded as identical, and can be given by a single description [see eqs. (17) and (18)], in the significant range of interest, $8 \leq B \leq 30$ dB. However, if the shallower fades are included ($0 \leq B \leq 8$ dB), there are, overall, more minimum phase fades (58 percent).

The Gainesville channel is more dispersive than the Palmetto chan-

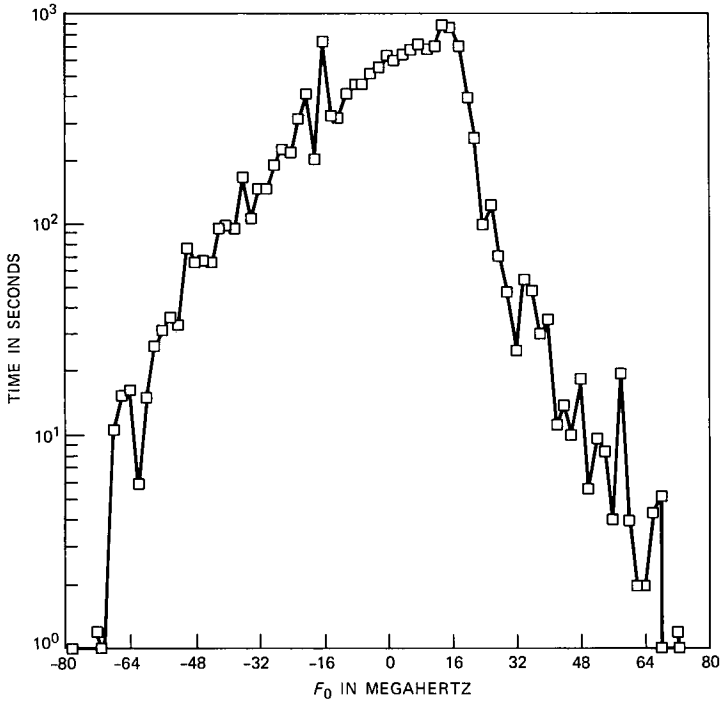

Fig. 19—Unnormalized probability density function of the notch frequency F_0 for the total population, measured from midband.

nel. This is seen from the estimated average annual distributions for the total fade populations. For the dispersive part of the fading, the B parameter, the distribution is steeper in Palmetto. By examining Fig. 16 for illustration purposes, we can deduce that there is five times more fading with $B = 20$ dB in Gainesville. In addition, the mean of A is smaller in Gainesville; $\bar{A}_G \approx 16$ dB, as compared with $\bar{A}_P \approx 26$ dB in Palmetto.

4.2 Implications in terms of performance objectives

AT&T long-haul digital-radio performance objectives limit service failure time to 0.02 percent (two way) annually on a 4000-mile route due to all causes. One-half of this is allocated to causes associated with equipment and maintenance. The allocation to dispersive fading, therefore, is 0.01 percent annually.[14] The one-way annual dispersive fading allocation for the average 25-mile hop is thus 10 seconds.

One measure of the amount of dispersive fading in a radio channel is the distribution of the parameter B. As seen from Fig. 16, a 10-second annual failure limit in Gainesville requires a robust digital radio system designed to operate with notches $B \leq 36$ dB. The same

failure limit in Palmetto requires a radio system designed to operate with notches of $B \leq 26$ dB. These comparisons demonstrate the need for a description of the geographical occurrence of dispersion, which will differ from that for multipath fading for a single frequency. The availability of such a dispersive fading map would facilitate the accurate engineering of digital radio routes.

V. ACKNOWLEDGMENTS

I would like to acknowledge the contributions of G. A. Axeling for aligning and maintaining the measurement equipment in Gainesville, B. J. Engelmann for utilizing her computer expertise to produce the statistical outputs, and G. L. Calhoun for maintaining the database. For many stimulating discussions on this work and comments on this manuscript, I would like to thank W. T. Barnett, L. J. Greenstein, V. K. Prabhu, W. D. Rummler, and A. Vigants.

REFERENCES

1. G. M. Babler, "A Study of Frequency Selective Fading for a Microwave Line-of-Sight Narrowband Radio Channel," B.S.T.J., *51,* No. 3 (March 1972), pp. 731–57.
2. L. J. Greenstein, "A Multipath Fading Channel Model for Terrestrial Digital Radio," IEEE Trans. Commun., *COM-26,* No 8 (August 1978), pp. 1247–50.
3. W. D. Rummler, "A New Selective Fading Model: Application to Propagation Data," B.S.T.J., *58,* No. 5 (May–June 1979), pp. 1037–71.
4. W. D. Rummler, "More on the Multipath Fading Channel Model," IEEE Trans. Commun., *COM-29,* No. 3 (March 1981), pp. 346–52.
5. L. J. Greenstein and B. A. Czekaj, "A Polynomial Model for Multipath Fading Channel Responses," B.S.T.J., *59,* No. 7 (September 1980), pp. 1197–225.
6. M. H. Meyers, "Multipath Fading Characteristics of Broadband Radio Channels," Globecom'84 Conf. Rec., *3* (November 1984), pp. 1460–5.
7. W. C. Jakes, Jr., "An Approximate Method to Estimate an Upper Bound on the Effect of Multipath Delay Distortion on Digital Transmission," IEEE Trans. Commun., *COM-27,* No. 1 (January 1979), pp. 76–81.
8. L. J. Greenstein and V. K. Prabhu, "Analysis of Multipath Outage With Applications to 90 Mbit/s PSK Systems at 6 and 11 GHz," IEEE Trans. Commun., *COM-27,* No. 1 (January 1979), pp. 68–75.
9. M. F. Gardina and A. Vigants, "Measured Multipath Dispersion of Amplitude and Delay at 6 GHz in a 30 MHz Bandwidth," ICC'84 Conf. Rec., *3* (May 1984), pp. 1433–6.
10. M. Liniger, "Sweep Measurements of Multipath Effects on Cross-Polarized RF-Channels Including Space Diversity," Globecom'84 Conf. Rec., *3* (November 1984), pp. 1492–6.
11. L. Martin, "Phase Distortions of Multipath Transfer Functions," ICC'84 Conf. Rec., *3* (May 1984), pp. 1437–41.
12. M. Sylvain and J. Lavergnat, "Modelling the Transfer Function of a 55 MHz Wide Radio Channel Multipath Propagation," ICC'85 Conf. Rec., June 1985, *3,* pp. 1541–6.
13. G. A. Axeling, private communication.
14. A. Vigants, "Space Diversity Engineering," B.S.T.J., *54,* No. 1 (January 1975), pp. 103–42.

AUTHOR

Philip Balaban, Diplom Ingenieur (Electrical Engineering), 1950, Technical University Munich; Ph.D. (Electrical Engineering), 1965, Polytechnic Insti-

tute of Brooklyn; Scientific Department, Israel, 1950–1956; Contraves, Zurich, Switzerland, 1956–1958; Computer Systems, New York, 1958–1962; Polytechnic Institute of Brooklyn, 1962–1967; AT&T Bell Laboratories, 1967—. Prior to joining AT&T Bell Laboratories, Mr. Balaban was engaged in research and development in the areas of circuit design, computers, and communications. At AT&T Bell Laboratories he worked on statistical modeling, simulation and analysis of transmission systems and circuits. Recently he has been involved with problems of channel characterization, and system performance of digital radio communication systems. In 1965–67 he taught at the Polytechnic Institute of Brooklyn, and in 1970–71 he was a visiting professor at the Technion in Israel. Senior Member, IEEE; Member, Sigma Xi.